High-Q Single Crystal Silicon HARPSS Capacitive Beam Resonators With Self-Aligned Sub-100-nm Transduction Gaps

Siavash Pourkamali, *Student Member, IEEE*, Akinori Hashimura, *Student Member, IEEE*, Reza Abdolvand, *Student Member, IEEE*, Gavin K. Ho, *Student Member, IEEE*, Ahmet Erbil, and Farrokh Ayazi, *Member, IEEE*

***Abstract*—This paper reports on the fabrication and characterization of high-quality factor (Q) single crystal silicon (SCS) in-plane capacitive beam resonators with sub-100 nm to submicron transduction gaps using the HARPSS process. The resonating element is made of single crystal silicon while the drive and sense electrodes are made of trench-refilled polysilicon, yielding an all-silicon capacitive microresonator. The fabricated SCS resonators are 20–40 μm thick and have self-aligned capacitive gaps. Vertical gaps as small as 80 nm in between 20 μm thick silicon structures have been demonstrated in this work. A large number of clamped-free and clamped–clamped beam resonators were fabricated. Quality factors as high as 177 000 for a 19 kHz clamped-free beam and 74 000 for an 80 kHz clamped–clamped beam were measured under 1 mtorr vacuum. Clamped–clamped beam resonators were operated at their higher resonance modes (up to the fifth mode); a resonance frequency of 12 MHz was observed for the fifth mode of a clamped–clamped beam with the fundamental mode frequency of 0.91 MHz. Electrostatic tuning characteristics of the resonators have been measured and compared to the theoretical values. The measured Q values of the clamped–clamped beam resonators are within 20% of the fundamental thermoelastic damping limits (Q_{TED}) obtained from finite element analysis. [950]**

***Index Terms*—Capacitive gap, HARPSS, quality factor, resonator, silicon micromachining, submicron, thermoelastic damping.**

I. Introduction

OVER the past few decades, development of silicon microfabrication technologies has provided the opportunity for batch fabrication of high-quality (Q) factor micromechanical resonators for a variety of sensing and frequency filtering applications. Due to the high sensitivity of the resonance frequency of micromechanical resonators to environmental parameters, these devices have great potential for implementation of highly sensitive resonant sensors such as pressure sensors, chemical sensors, accelerometers and gyroscopes. In addition to the sensory applications, extreme demand for high-performance highly-integrated wireless communication units has fueled interest in replacing the off-chip bulky frequency selective components in communication systems with integrated micromechanical resonant devices [1]. However, extension of the operating frequency of capacitive MEMS resonators to the VHF and UHF range requires ultra-thin capacitive gaps as small as a few 10's of nanometers in between the electrodes and the high Q resonating element [2]. Therefore, fabrication technologies that can implement all-silicon high-Q capacitive resonators with scalable nanometer-in-size gap spacing without the need for nanolithography are of great interest.

A variety of micromechanical resonators with single crystal or polycrystalline silicon as the structural material have been so far reported in literature. Surface micromachined polysilicon capacitive resonators with submicron gap spacing have been demonstrated [3], [4]. Single crystal silicon (SCS) is a more attractive structural material for microresonators compared to polysilicon due to its low internal friction and consequently higher mechanical Q, low internal stress and independence from various process parameters. However, fabrication of electrically-isolated single crystal silicon mechanical structures with very small gaps introduces several problems and limitations. Silicon-on-insulator (SOI) substrates [5]–[7] or wafer bonding techniques [8], [9] are usually used for implementation of SCS devices resulting in higher cost and process complexity. The single crystal silicon resonators that have been so far reported in literature use fabrication processes that are not capable of producing sense and drive electrodes in sub-100 nm proximity of the resonant structure. They either have complex optical [6], [7], [10] or magnetic [11] sense and actuation scheme or, in case of capacitive resonators, the gaps cannot be scaled down to sub 100-nm level using optical lithography [5], [8], [12], limiting their application to low frequencies.

This paper presents the implementation and characterization of high-Q in-plane SCS capacitive beam resonators with sub-100 nm to submicron transduction gaps using the HARPSS process. An enhanced and modified version of the HARPSS (High Aspect Ratio combined Poly and Single crystal Silicon) process [13], [14] has been used in this work to fabricate 10's of microns thick SCS resonators within submicron vicinity of vertical polysilicon electrodes [15]. Sub-100 nm self-aligned vertical capacitive gaps are demonstrated for the first time in 20 μm thick SCS capacitive resonators. Thick in-plane resonators

Manuscript received October 24, 2002; revised January 14, 2003. This work was supported by DARPA under Contract DAAH01-01-1-R004. Subject Editor G. B. Hocker.

S. Pourkamali, R. Abdolvand, G. K. Ho, and F. Ayazi are with the School of Electrical and Computer Engineering, Georgia Institute of Technology Atlanta, GA 30332-0250 USA (e-mail: ayazi@ece.gatech.edu).

A. Hashimura was with the School of Electrical and Computer Engineering, Georgia Institute of Technology Atlanta, GA 30332-0250 USA. He is now with Panasonic, Osaka, Japan.

A. Erbil is with the School of Physics, Georgia Institute of Technology Atlanta, GA 30332-0250 USA.

Digital Object Identifier 10.1109/JMEMS.2003.811726

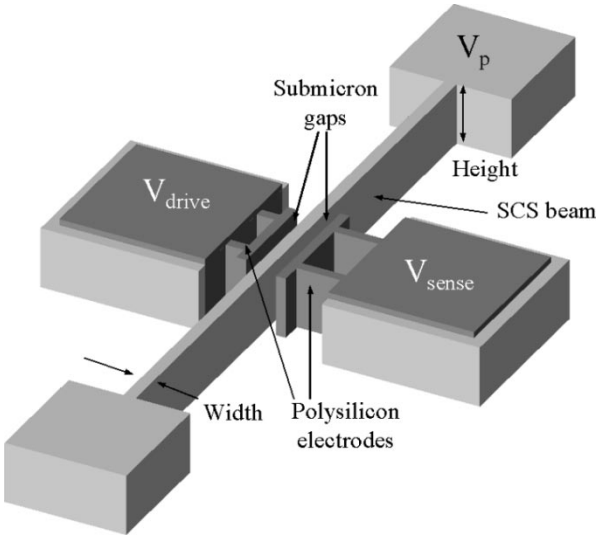

Fig. 1. Schematic view of a two-port clamped–clamped SCS beam resonator fabricated through the HARPSS process.

have the advantage of consuming smaller die area by extending in the vertical direction into the silicon substrate. This provides larger drive and sense area, which when combined with the ultra small gaps will reduce the equivalent motional resistance of the resonator (increase the signal to noise ratio). Measurement results on the Q of clamped–clamped and clamped-free SCS beams with various dimensions operating in their fundamental and higher order flexural modes are reported and compared to the theoretical values. Tuning characteristics of the fabricated beam resonators in the fundamental and higher order modes are also presented. It is shown through finite-element analysis that the measured Q's of the clamped–clamped beam resonators are very close to the fundamental thermoelastic damping limits (Q_{TED}).

II. Resonator Fabrication

The HARPSS process has been previously used to fabricate thick trench-refilled polysilicon resonators and gyroscopes [14]. In this work, a modified version of the HARPSS process is deployed to implement 10's of microns thick single crystal silicon resonating structures with thick polysilicon electrodes [15]. The schematic diagram of an in-plane two-port clamped–clamped beam resonator fabricated through the HARPSS process is shown in Fig. 1.

As shown in Fig. 2, the fabrication process starts by defining the electrically isolated bonding pads for the electrodes. A 1 μm thick silicon dioxide covered by a thin layer of LPCVD silicon nitride (3000°A) is used to create the bonding pads [see Fig. 2(a)]. To define the SCS resonating beam, two adjacent high aspect-ratio trenches (5 μm wide and 20–40 μm deep) are etched into the low-resistivity silicon substrate using a deep-reactive ion etching (DRIE) system. The height of the trenches determines the height of the resonator. A thin conformal layer of high-temperature LPCVD oxide is then deposited $(\sim 850^{\circ}\ \mathrm{C})$ [see Fig. 2(b)] and trenches are subsequently refilled with doped LPCVD poly to form the vertical electrodes. The lateral gap spacing is defined by the thickness of the deposited oxide layer. Polysilicon is etched back on the surface using plasma etching to expose the sacrificial oxide layer [see Fig. 2(c)]. Sacrificial oxide is then patterned and another doped LPCVD layer of polysilicon is deposited. Polysilicon is patterned to form the pads followed by metallization using $\mathrm{Cr}(200^{\circ}\mathrm{A})/\mathrm{Au}(2000^{\circ}\mathrm{A})$ [see Fig. 2(d)]. The resonator is released from the silicon substrate using a dry silicon etch in SF6 plasma, consisting of an anisotropic followed by an isotropic etch to undercut the structures [see Fig. 2(e)]. During the isotropic etch step the sacrificial oxide layer protects the silicon structure and polysilicon electrodes. Finally, the sacrificial oxide is removed in a $\mathrm{HF}\ :\ \mathrm{H_2O}$ (1:1) solution to release the structures [see Fig. 2(f)]. Various types of capacitive resonator with different dimensions covering a wide frequency range can be fabricated using this process technology. Fig. 3 shows the SEM picture of fabricated clamped–clamped and clamped-free SCS HARPSS beam resonators. Figs. 4 and 5 are the SEM pictures of the electrode area, showing the single crystal beam, the polysilicon electrodes and the submicron gap in between.

A. Sub-100-nm Capacitive Gaps

The self-aligned nature of the gap formation in between the SCS and trench-refilled polysilicon structures in the HARPSS process allows for the reduction of the capacitive gaps to the tens of nanometer range. Single crystal silicon resonators with capacitive gaps as small as 80 nm have been fabricated in this work. Fig. 6 shows SEM pictures of the cross section of 200 nm and 80 nm uniform vertical gaps in between the polysilicon inside the trench and the silicon substrate. Top view of the clamped–clamped beam resonators with 80 nm drive and sense capacitive gaps and the close-up view of the electrode area are shown in Fig. 7. This device has been successfully operated and the results are presented later in this paper.

B. Polysilicon Electrode Definition

In this process, the trenches are used to define: 1) the boundary of the resonating structure, and 2) the polysilicon electrodes. At the end of the process (during the dry release step), all the polysilicon inside the trenches is removed, except for the electrode area. To separate and protect the polysilicon in the electrode area from the areas that only define the boundary of the resonator, two methods were investigated which are shown in Fig. 8(a) and (b). The first method is to physically disconnect the polysilicon electrode by using discontinuous trenches and etch away the polysilicon inside the trenches that define the boundary of the resonator. However, this method creates "stubs" on the sides of the beam as shown in the SEM of Fig. 8(a), introducing residual extra mass and uncertainty in the operating frequency of the resonators. Finite element analysis using ANSYS have shown that these stubs do not alter the resonance frequency significantly. The size of these stubs can be controlled by characterizing the timing of isotropic release etch step. The alternative method is to use a continuous trench to define the boundary of the resonator and reduce the width of the trench in certain areas between the electrode trench and the trenches that only define the shape. The narrow trench located in between the regular size trenches will be refilled by oxide only; this will subsequently create a barrier to the $\mathrm{SF_6}$

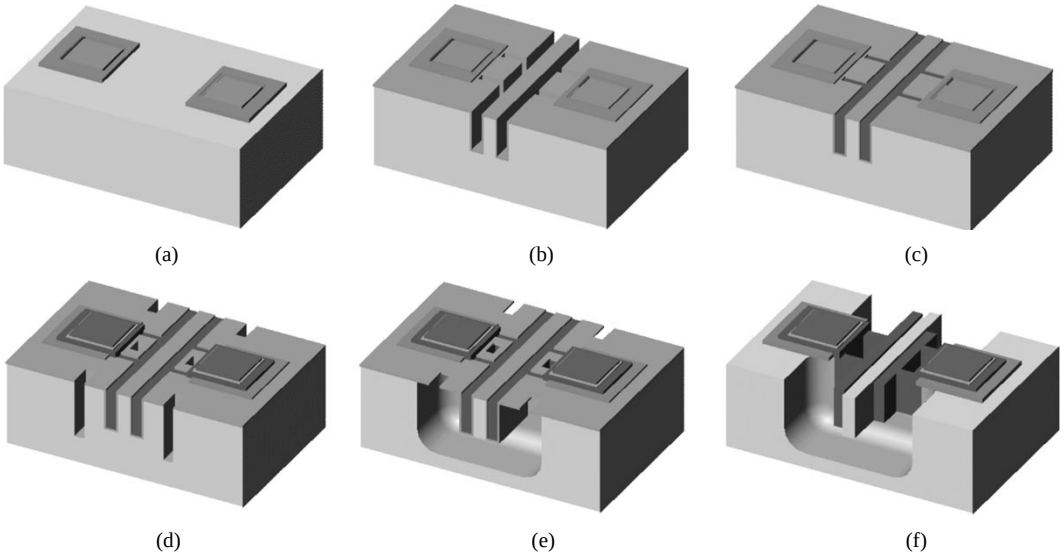

(a) (b) (c)

(d) (e) (f)

Fig. 2. HARPSS fabrication process flow for single crystal silicon beam resonators.

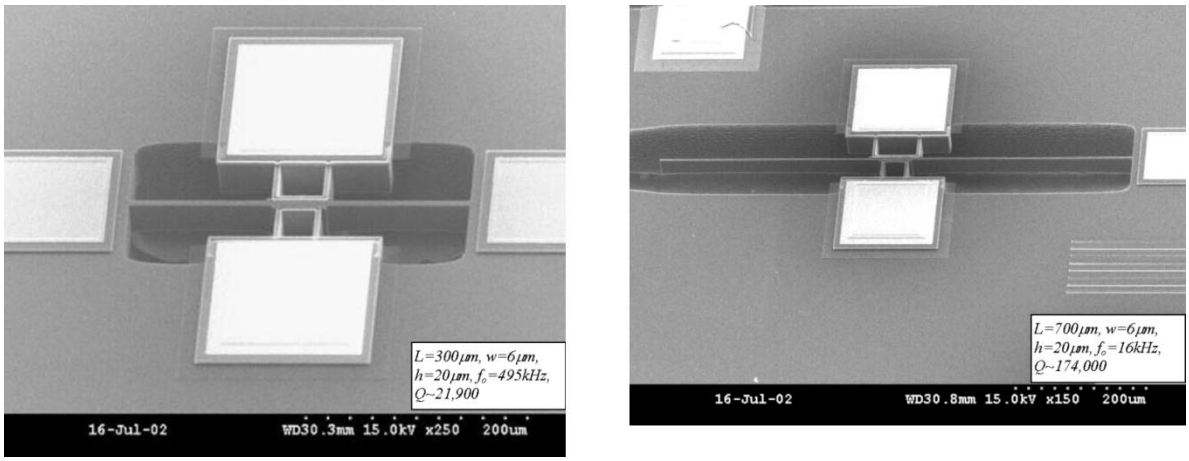

(a) (b)

Fig. 3. SEM view of (a) clamped–clamped and (b) clamped-free single crystal silicon beam resonators fabricated through the HARPSS process.

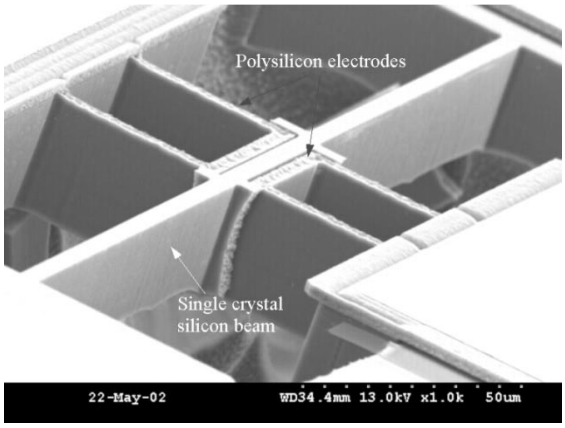

Fig. 4. SEM of the electrode area showing the polysilicon electrodes as tall as the beam separated by submicron gaps.

flow to protect the polysilicon electrodes as shown in Fig. 8(b). It should be noted that, due to the presence of voids in the middle of the narrow trenches, a thin residual poly line might be formed, connecting the electrode poly to the boundary poly. This parasitic polysilicon results in larger effective electrode area and will be subsequently etched away during the isotropic etch step.

III. Measurement Results

Fabricated SCS beam resonators were tested under vacuum in a two-port configuration using an Agilent 4395A network analyzer. The sensing interface circuits were assembled on a printed circuit board (PCB) using surface mount components. The MEMS resonator chip was mounted on the board and the input and output signals along with the dc polarization voltage were applied to the resonator through wire-bonds. The PCB was placed inside a custom vacuum system, which keeps the pressure below 1 mtorr. Fig. 9 shows a schematic diagram of the setup for testing the resonators. Two different sense circuit configurations were used for testing the resonators. A J-FET input high frequency operational amplifier was connected in 1) noninverting voltage amplifier and 2) inverting trans-resistance configuration. Both circuit configurations are capable of detecting

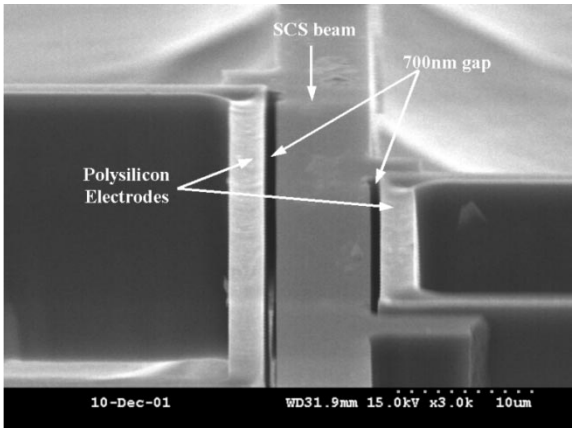

Fig. 5. Close-up view of the electrode area showing the 700 nm gap spacing.

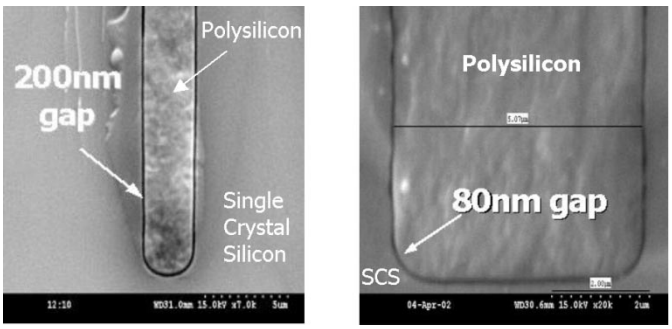

(a) (b)

Fig. 6. Cross-sectional SEM view of trench refilled with polysilicon separated from the substrate with (a) 200 nm and (b) 80 nm uniform gaps.

the small output current of the resonators (in the range of a few nA).

A. Fundamental Mode Results

Fig. 10 shows the plot of a typical frequency response taken from the network analyzer, showing a Q of 74 000 at 80 kHz for a 700 μm long, 6 μm wide and 20 μm tall SCS clamped–clamped beam resonator under 1 mtorr vacuum. The summary of the Q measurement results for the clamped–clamped beam resonators with various fundamental resonance frequencies ranging from 41.5 kHz to 3.2 MHz is given in Table I. The Q decreases as the frequency of the beam increases. A Q of $\sim$ 4500 was measured for the 3.2 MHz beam resonator.

Significantly higher quality factors are measured for clamped-free beams due to their lower resonance frequency and reduced support loss. A quality factor of 177 000 has been measured for a 500 μm long, 4 μm wide SCS clamped-free beam resonator at the center frequency of 19 kHz (see Fig. 11). Table II presents measured quality factors for clamped-free beams with different dimensions.

B. Frequency Tuning

Resonance frequency of parallel plate capacitive resonators can be tuned by changing the dc polarization voltage applied across the sense and drive capacitive gaps. As the resonator vibrates variations in the resonator to electrode distances result in force components at the resonance frequency that oppose the force produced by the mechanical stiffness of the structure. This effect can be modeled by an equivalent negative electrical stiffness as expressed in (1) that partly cancels the mechanical stiffness and reduces the resonance frequency of the resonator

$$K_{\text{elec}} = -\frac{V_p^2 C_{do}}{d_d^2} - \frac{V_p^2 C_{so}}{d_s^2} \tag{1}$$

where V_p is the dc polarization voltage applied between the electrodes and the resonator, C_{do} and C_{so} are the capacitances between the beam and the drive and sense electrodes, respectively, and d_d and d_s are the drive and sense capacitive gaps.

Fig. 12 shows the comparison between the measured and theoretical frequency tuning characteristics for a 300 μm long, 6.5 μm wide resonator with 700 nm capacitive gaps by changing the dc polarization voltage (Vp). The mismatch is mainly due to uncertainties in the resonator structure caused during the isotropic etch step to undercut the structure, which alter the overall stiffness of the beam. The resonance frequency changed from 505 to 450 kHz by changing the polarization voltage by more than 40 V (the calculated pull-in voltage was 56 V), providing a large electrostatic tuning range ($\sim$ 10%).

C. Sub-100-nm Gap Resonators

The capability of HARPSS to implement resonators with sub-100-nm capacitive gaps was shown by the successful characterization of the 80 nm gap device of Fig. 7. Fig. 13 shows the frequency response of the 610 kHz resonator with 80 nm sense and drive gaps, demonstrating a Q of 4800 under vacuum. Much larger tuning range and significantly sharper tuning characteristic are observed for the devices with sub-100-nm capacitive gaps. Measured tuning characteristic of the 610 kHz clamped–clamped beam resonator with 80 nm capacitive gaps is shown in Fig. 14, demonstrating a tuning range of 28% by changing the polarization voltage from 0.1 to 2.0 V. The results are in good agreement with theory.

D. Higher Resonance Modes

In order to achieve higher operating frequencies without reducing the size of the structures, resonators can be operated in their higher resonance modes. The natural frequencies of clamped–clamped beam resonators are given by (2) [16]

$$f_n = \frac{\lambda_n^2}{2\pi L^2}\sqrt{\frac{EI}{M}} \tag{2}$$

where L is the length of the beam, E is the Young's modulus of the beam material, I is the area moment of inertia around the principal axis, M is the mass of the beam and λ_n is the frequency coefficient for each resonance mode that can be calculated by solving (3)

$$\text{Cos}\lambda_n \text{Cosh}\lambda_n = 1. \tag{3}$$

For a clamped–clamped (C–C) beam, λ_n values for the first, third and fifth resonance modes are $\lambda_1 = 4.730$, $\lambda_3 = 11.11$ and $\lambda_5 = 17.28$, respectively. Therefore, the third and fifth modes should have resonance frequencies of 5.52 and 13.3 times higher than the fundamental mode, respectively.

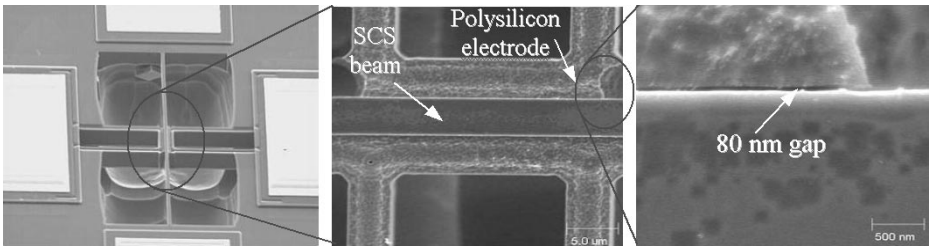

Fig. 7. Top view of the 600 kHz single crystal silicon resonator and close-up view of the electrode area showing the 80 nm gap spacing.

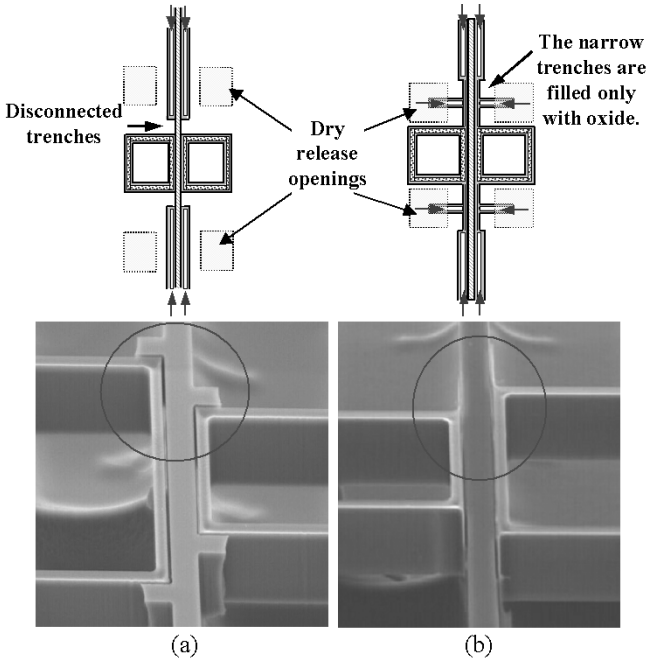

Fig. 8. Diagram and SEM of the separation methods using (a) disconnected trenches and (b) narrow trenches.

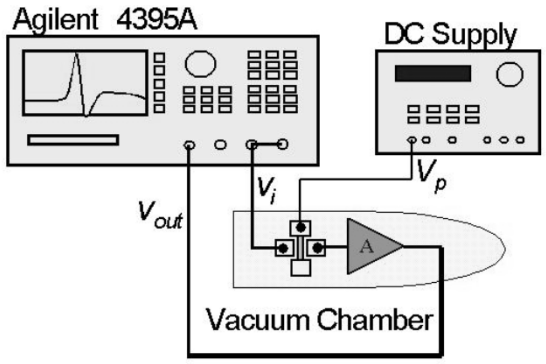

Fig. 9. Test setup for measurement of resonator frequency response.

Fabricated C-C beam resonators were excited in their third and fifth flexural modes and the quality factors were measured. The second and the fourth modes could not be excited due to the midway position of the drive electrode. Resonance frequencies up to 12.0 MHz have been achieved by exciting the fifth resonance mode of a 200 μm long 5 μm wide clamped–clamped beam with the fundamental resonance frequency of 910 kHz. Fig. 15 shows the measured resonance peaks and Q values for various modes of this resonator. A summary of measured center frequencies and quality factors for clamped–clamped beams in

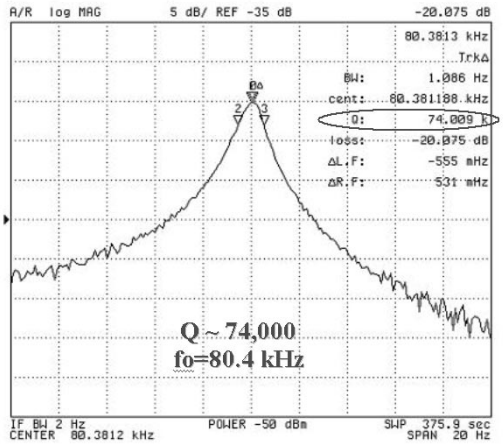

Fig. 10. Frequency response of a 700 μm long, 5μm wide, 20 μm thick clamped–clamped beam resonator.

TABLE I
MEASUREMENT RESULTS ON RESONANCE FREQUENCY AND QUALITY FACTOR OF THE VARIOUS SCS CLAMPED–CLAMPED BEAM RESONATORS FABRICATED THROUGH HARPSS TECHNOLOGY

Dimensions		f-1st (kHz)	Q
W(μm)	L (μm)		
5	700	80.3	74,000
7.5	700	125.5	39,400
4	500	117.0	67,000
5.5	500	164.5	60,400
6.5	500	198.0	35,000
7.5	500	217.0	27,000
4	300	288.4	43,000
5.5	300	489.3	21,500
6	300	495.5	21,900
6.5	300	528.0	17,000
5	200	911	10,000
10	200	3200	4,500

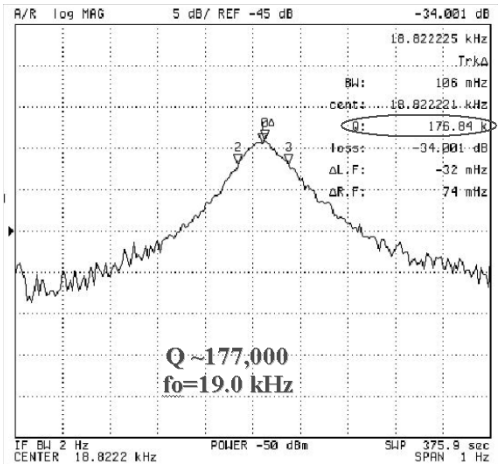

Fig. 11. Frequency response of a 500 μm long, 4 μm wide, 20 μm thick clamped-free beam resonator.

TABLE II
MEASUREMENT RESULTS ON RESONANCE FREQUENCY AND QUALITY FACTOR OF THE VARIOUS SCS CLAMPED-FREE BEAM RESONATORS FABRICATED THROUGH HARPSS TECHNOLOGY

Dimensions		f-1st (kHz)	Q
W (μm)	L (μm)		
6.5	700	15.94	173,800
4	500	19.00	178,000
5	500	24.59	157,400
6	500	30.14	154,800

their higher resonance modes is presented in Table III. Measured frequencies for higher resonance modes are in good agreement with the values predicted by (2). Due to higher stiffness of the beams in higher modes, excitation of resonators in those modes requires higher polarization voltages or smaller excitation and sense gaps. For the same reason, tuning capability at higher resonance modes is weaker than the fundamental modes. Fig. 16 shows tuning characteristics of a 300 μm long, 5 μm wide clamped–clamped beam with 700 nm gaps at its third resonance mode showing a tuning slope of 0.18 kHz/V, which is significantly lower than that of the first resonance mode of such resonator (2.5 kHz/V).

Comparison of the measured quality factor values for the fundamental and higher resonance modes shows that at a certain center frequency and beam width measured Q for beam resonators at higher order modes are equal or even slightly greater than that of the fundamental resonance modes (see Fig. 17).

As shown in Table I, the Q of the fabricated HARPSS C-C beam resonators decreases as the frequency of the beam resonator increases. This trend is similar to what is predicted by the thermoealstic damping (TED) loss. However, to verify the results and benchmark the HARPSS process as an enabling technology for "high-Q" capacitive SCS resonators, the fundamental TED-based limits of the quality factor for the fabricated

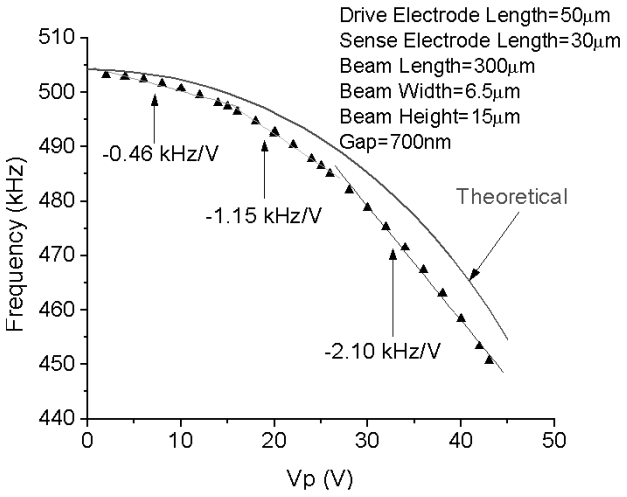

Fig. 12. Plots of measured and calculated change of frequency versus polarization voltage for a 500 kHz clamped–clamped beam resonator with 700 nm capacitive gaps.

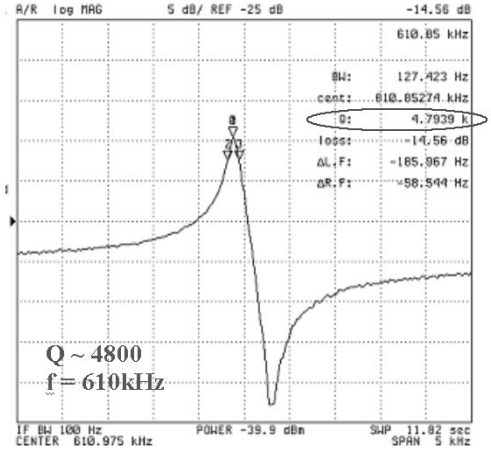

Fig. 13. Frequency response of a 200 μm long, 3 μm wide, 20 μm thick clamped-free beam resonator with 80 nm capacitive gaps.

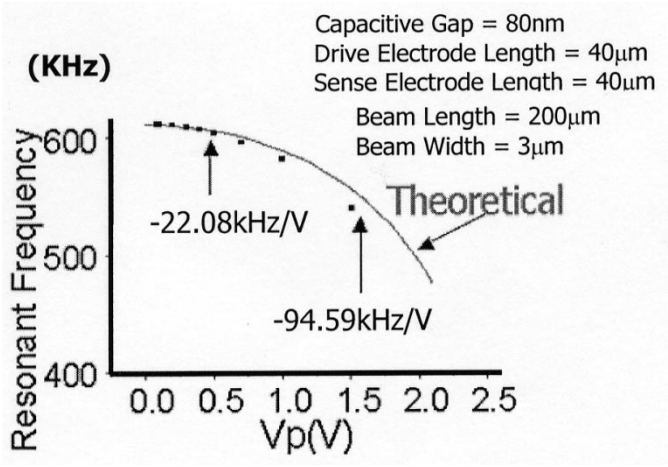

Fig. 14. Plots of measured and calculated change of frequency versus polarization voltage for a 610 kHz clamped–clamped beam resonator with 80 nm capacitive gaps.

resonators were computed and compared to the measurement results. The results are presented in the next section.

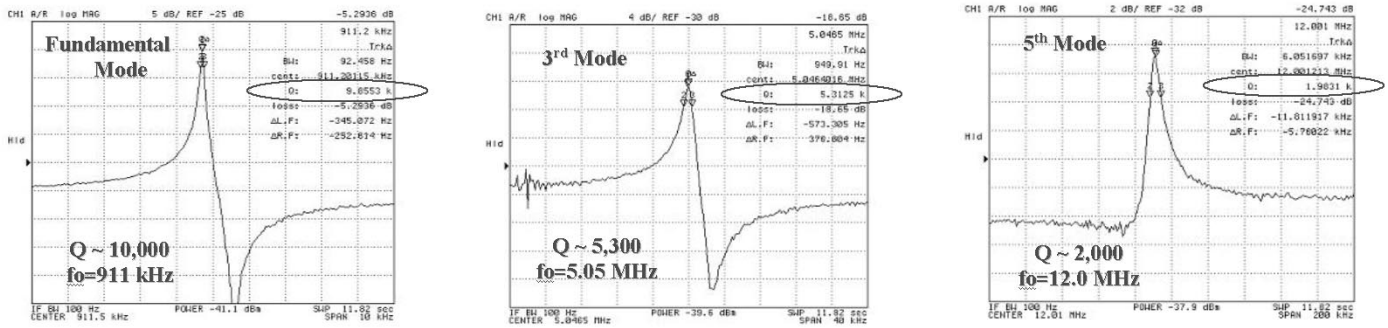

(a) (b) (c)

Fig. 15. Frequency response of a 200 μm long, 5 μm wide, 20 μm thick with capacitive 200 nm capacitive gaps at fundamental, third and fifth resonance modes.

TABLE III
MEASUREMENT RESULTS ON RESONANCE FREQUENCY AND QUALITY FACTOR OF THE VARIOUS SCS CLAMPED–CLAMPED BEAM RESONATORS AT FUNDAMENTAL AND HIGHER RESONANCE MODES

Dimension		f_0-1st (kHz)	f_0-3rd (MHz)	Q 3rd	f_0-5th (MHz)	Q 5th
W (_m)	L (_m)					
7.5	900	74.8	0.44	10,400	-	-
5	700	80.3	0.49	23,100	1.24	10,700
7.5	700	125	0.74	8,000	-	-
5	500	116	0.72	21,300	1.88	7,600
5.5	500	165	1.03	10,700	-	-
6.5	500	198	1.21	8,300	-	-
4	300	288	1.71	13,900	4.41	8,400
6	300	496	2.72	6,700	-	-
5	200	911	5.05	5,000	12.0	2,000

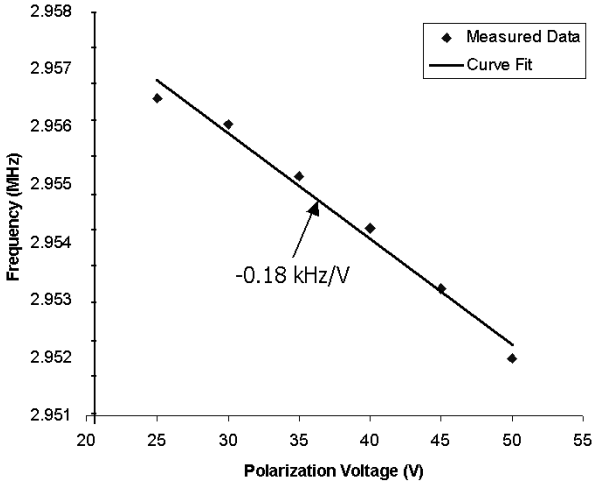

Fig. 16. Tuning characteristic of a 300 μm long, 5 μm wide clamped–clamped beam with 700 nm gaps at its third resonance mode.

IV. LOSS MECHANISMS

Various loss mechanisms in beam resonators have been investigated by researchers including the thermoelastic damping (TED), support, and surface related losses [7], [12], [17]–[20].

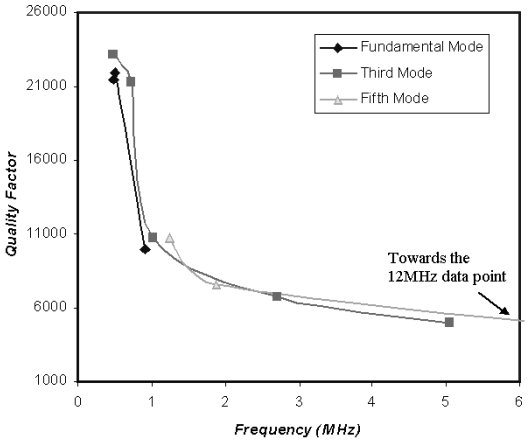

Fig. 17. Comparison of measured quality factors for fundamental, third and fifth resonance modes for resonators with width of 5 to 6 μm.

Among these, the thermoelastic damping could be the most significant loss mechanism in flexural beam resonators with large aspect ratios [12], [17], [20]. Thermoelastic damping is a result of irreversible heat flow across temperature gradients produced by inhomogeneous compression and expansion of the oscillating beam. Here we present the results of a finite element analysis (FEA) to establish the limitations imposed on the quality factor by the TED mechanism. The finite element method can handle realistic device geometries without the simplifying assumptions that are often made in analytical methods to reach closed form expressions [18], [21].

The thermoelastic damping mechanism is governed by the following coupled partial differential equations:

$$p\ddot{u}_i - \frac{E}{2(1+\sigma)}\frac{\partial^2 u_i}{\partial x_k^2} - \frac{E}{2(1+\sigma)(1-2\sigma)} \times \frac{\partial^2 u_1}{\partial x_i \partial x_l} = -\frac{E\alpha}{3(1-2\sigma)}\frac{\partial T}{\partial x_i} \tag{4}$$

and

$$C_v\frac{\partial T}{\partial t} - \nabla\cdot(k\nabla T) = -\frac{E\alpha T_0}{3(1-2\sigma)}\frac{\partial}{\partial t}\frac{\partial u_i}{\partial x_i} \tag{5}$$

where we assume summation over the repeated indices. The departure of the beam elements from equilibrium are described by a displacement field $u_i(i = x, y, z)$ and T denotes the temperature field. The terms on the right hand sides provide coupling between (4) and (5). The equation parameters and the values used

TABLE IV
DEFINITION OF PARAMETERS IN THE COUPLED THERMAL AND STRAIN FIELD EQUATIONS

Parameter	Notation	Value
Density	ρ	2330 kg/m^3
Young's Modulus for Si [100]	E	1.3×10^{11} GPa
Poisson's Ratio for Si [100]	σ	0.28
Volume Expansion Coefficient	α	7.8×10^{-6} /K
Specific Heat per Unit Volume	C_v	1.63×10^6 J/K-m^3
Thermal Conductivity	k	90 W/m-K
Beam Uniform Temperature	T_0	300 K

in our simulation are provided in Table IV. In equilibrium, the beam is unstrained and unstressed, and has a uniform temperature of T_0. The value for thermal conductivity was taken from the experimental plots given in [22] for a p-type low-resistivity silicon substrate with doping levels in excess of $2 \times 10^{19}\text{cm}^{-3}$.

The multiphysics TED simulation for the clamped–clamped beam resonators was performed by using the FEMLAB [23] software. Since the width of the beams is much smaller that the other two dimensions, a plane-strain assumption was made to reduce the computation time. A three-dimensional analysis yields the same results within the uncertainties of the experiment. For a given resonator, the amplitude at the midpoint was calculated as a function of driving frequency. The response curve was fit to a lorentzian function to obtain the quality factor Q.

Fig. 18(a) and (b) show the results of FEA along with the experimental data points for C-C beams that are 5.0 μm and 7.5 μm wide, respectively. For each FEA plot, only the length of the beam was changed to obtain different resonant frequencies. The solid circles show the points obtained from FEA for the first harmonic, and the solid line is drawn as a guide to the eye. The measurements for both first and third harmonic quality factors for various beams are shown for comparison. The agreement between the measurement and the FEA prediction is excellent, and within the uncertainties of the measurements in both Fig. 18(a) and (b). The analytical predictions by Lifshitz and Roukes [18] are also shown on the figures for comparison (dashed lines). The resonator parameters were kept the same as the ones used for the FEA. The analysis by Lifshitz and Roukes [18] consistently overestimates the Q values predicted by FEA by a factor of about two, which might be due to the simplifying assumptions. It should be noted that the FEA for the third harmonic was also performed in FEMLAB and the results were within 5% of the first harmonic FEA Q values for the same width beam (the plot for the third harmonic FEA was not added for the sake of legibility).

Support loss of clamped-free (C-F) beam resonators has been studied in [7] and [19], and the following expression [see (6)] was derived for Q_{support}:

$$Q_{\text{sprt}} \approx 2.17 \left(\frac{L}{w}\right)^3 \tag{6}$$

where L and w are length and width of the C-F beam, respectively, and the resonator and support are of the same material.

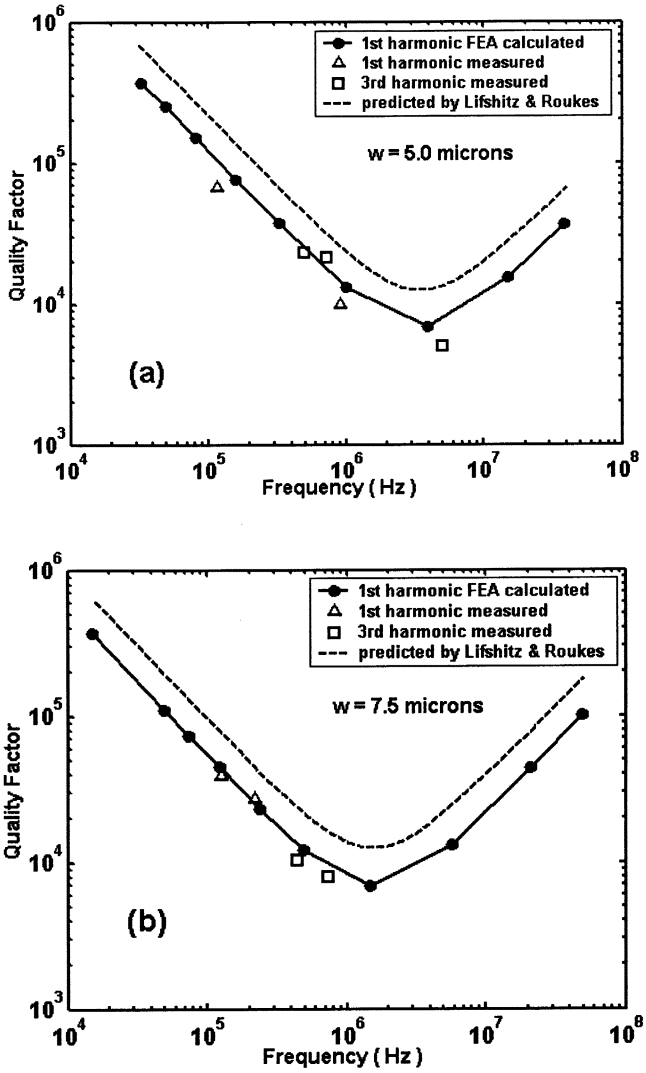

Fig. 18. Measurement results of Q for beams of several thicknesses (regardless of mode number) plotted versus frequency in comparison with the theoretically predicted QTED.

The expression for support loss of a clamped–clamped beam is expected to have similar geometrical dependency with a different proportionality factor. For the resonators studied in this work with fundamental frequencies below 1 MHz, the large length to width ratios of the resonators $(L/w > 40)$ result in larger Q_{support} than the measured Q values, indicating that support loss cannot be the major Q limiting mechanism. However for some of the higher order resonance modes of the beams, support loss can become the dominant loss mechanism.

To investigate the significance of surface related losses [12] in the Q of the fabricated beam resonators, two different batches of resonators were fabricated and characterized. For the second batch, after etching the trenches that define the boundary of the SCS beams, a thin layer of thermal oxide $(\sim 3500\,\text{Å})$ was grown on the Si surfaces and subsequently removed by wet etching in buffered HF solution. The first batch did not undergo this oxidation treatment. As shown in Fig. 19, the thermal oxidation substantially reduced the roughness of the SCS beam sidewalls (introduced during the unoptimized DRIE etch process). Measurement results obtained from the two batches of the resonators

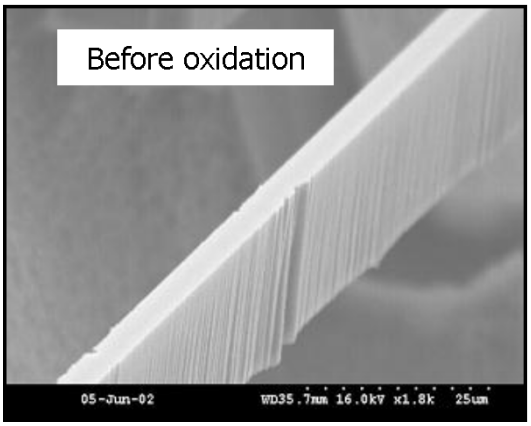

(a)

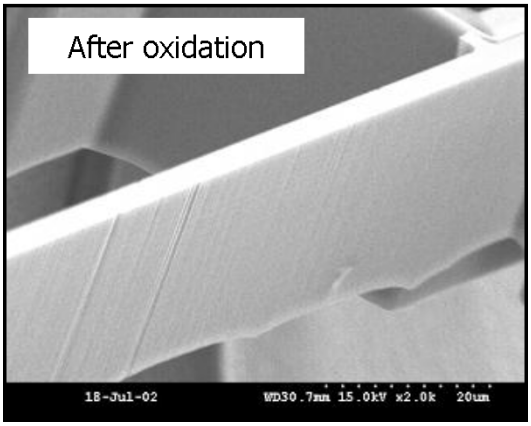

(b)

Fig. 19. SEM pictures showing surface roughness of beam sidewalls before oxidation step (a) and its improvement after thermal oxidation and oxide removal (b).

revealed that the surface oxidation treatment provides only a slight improvement of about 15–20% in the Q values. Therefore, considering the fact that the measured Q values are within 20% of the fundamental Q_{TED} values, we conclude that surface related losses are not a major source of loss in the fabricated HARPSS SCS resonators.

V. Conclusion

All-silicon high-Q capacitive micromechanical beam resonators with sub-100 nm to submicron gap-spacing utilizing single crystal silicon as the resonating element and polysilicon as the electrodes have been reported. The resonators were fabricated using the HARPSS process in which capacitive gaps are defined in a self-aligned process by the thickness of the deposited sacrificial layer. Uniform vertical capacitive gaps of 80 nm are demonstrated without the need for nanolithography. Measurement results for several beam dimensions operating in different resonance modes have been reported. Quality factors as high as 177 000 for a clamped-free beam at 19 kHz, and resonance frequencies as high as 12 MHz for the 5^{th} flexural mode of a clamped–clamped beam with Q of 2000 have been achieved. The possibility of operation of beam resonators in their higher resonance modes with high quality factors has been demonstrated. Investigation of various loss mechanisms revealed that the measured quality factors for compliant high-aspect-ratio beams follow the behavior predicted by the TED loss mechanism.

Acknowledgment

The authors wish to thank S. Y. No for his contributions and the staff of Georgia Tech Microelectronics Research Center, especially the CMOS group, for their assistance.

References

[1] C. T.-C.Clark T.-C. Nguyen, "Micromechanical circuits for communication transceivers," in *Bipolar/BiCMOS Circuits and Technology Meeting (BCTM)*, 9 25–26, 2000, pp. 142–149.

[2] S. Y. No and F. Ayazi, "The HARPSS process for fabrication of nano-precision silicon electromechanical resonators," in *Proc. IEEE Conf. on Nanotechnology*, 10 28–30, 2001, pp. 489–494.

[3] W.-T. Hsu *et al.*, "Q-optimized lateral free-free beam micromechanical resonators," in *Proc. Int. Conf. On Solid-State Sensors and Actuators (Transducer'01)*, Munich, Germany, 6 10–14, 2001, pp. 1110–1113.

[4] K. Wang, A. C. Wong, and C. T.-C. Nguyen, "VHF free-free beam high-Q micromechanical resonators," *J. Microelectromech. Syst.*, vol. 9, pp. 347–360, Sept. 2000.

[5] T. Mattila *et al.*, "14 MHz micromechanical oscillator," in *Proc. 11th Int. Conf. on Solid-State Sensors and Actuators, (Transducer'01)*, Munich, Germany, 6 10–14, 2001, pp. 1102–1105.

[6] S. Kobayashi *et al.*, "Shape effect on mechanical quality factor of microresonator," in *Proc. MEMS 98*, pp. 195–200.

[7] K. Y. Yasumura *et al.*, "Quality factors in micron- and submicron-thick cantilevers," *J. Microelectromech. Syst.*, vol. 9, p. 117, Mar. 2000.

[8] K. Petersen *et al.*, "Resonant beam pressure sensor fabricated with silicon fusion bonding," in *6th Int. Conf. on Solid State Sensors and Actuators, (Tranducer'91)*, San Francisco, CA, 6 24–28, 1991, pp. 664–667.

[9] R. A. Buser and N. F. De Rooij, "Capacitively activated torsional high-Q resonator," in *An Investigation of Micro Structures, Sensors, Actuators, Machines and Robots*: IEEE, 1990, pp. 132–135.

[10] ——, "Very high Q-factor resonators in monocrystalline silicon," *Sens. Actuators*, pp. A21–A23, 1990.

[11] A. N. Cleland and M. L. Roukes, "Fabrication of high frequency nanometer scale mechanical resonators from bulk Si substrates," *App. Phys. Lett.*, vol. 69, p. 2653, 1996.

[12] R. E. Mihailovich and N. C. MacDonald, "Dissipation measurements of vacuum-operated single-crystal silicon microresonators," *Sens. Actuators A*, vol. 50, p. 199, 1995.

[13] F. Ayazi and K. Najafi, "High Aspect-Ratio Combined Poly and Single-Crystal Silicon (HARPSS) MEMS technology," *J. Microelectromech. Syst.*, vol. 9, p. 288, Sept. 2000.

[14] ——, "A HARPSS polysilicon vibrating ring gyroscope," *J. Microelectromech. Syst.*, pp. 169–179, June 2001.

[15] S. Y. No, A. Hashimura, S. Pourkamali, and F. Ayazi, "Single crystal silicon HARPSS capacitive resonators with submicron gap spacings," in *Proc. Hilton Head 2002, Solid-State Sensor, Actuator and Microsystems Workshop*, pp. 281–284.

[16] R. D. Blevins, *Formulas for Natural Frequency and Mode Shape*. New York: Van Nostrand Reinhold, 1979.

[17] T. V. Roszhart, "The effect of thermoelastic internal friction on the Q of micromachined silicon resonators," in *IEEE Solid State Sensor and Actuator Workshop*, Hilton Head, SC, 6 4–7, 1990, pp. 489–494.

[18] R. Lifshitz and M. L. Roukes, "Theromoelastic damping in micro- and nanomechanical systems," *Phy. Rev. B.*, vol. 61, no. 8, p. 5600, 2000.

[19] Y. Jimbo and K. Itao, "Energy loss of a cantilever vibrator," *Journal of the Horological Institute of Japan*, 1968.

[20] A. Duwel, M. Weinstein, J. Gorman, J. Borenstein, and P. Ward, "Quality factors of MEMS gyros and the role of thermoelastic damping," in *Proc. Fifteenth IEEE International Conference on Micro Electro Mechanical Systems*, 2002, pp. 214–219.

[21] J. Gorman, "Finite Element Model of Thermoelastic Damping in MEMS," Master of Science Thesis, Department of Materials Science, Massachusets Institute of Technology, May 2002.

[22] M. Asheghi, K. Kurabayashi, R. Kasnavi, and K. E. Goodson, "Thermal conduction in doped single-crystal silicon films," *Journal of Applied Physics*, vol. 91, no. 8, pp. 5079–5088, April 2002.

[23] *FEMLAB Multiphysics in MATLAB*. Burlington, MA, USA: COMSOL, Inc.

Siavash Pourkamali (S'03) was born in 1980. He received the B.S. degree in electrical engineering from Sharif University of Technology, in 2001. Currently, he is working towards the Ph.D. degree at the Electrical Engineering Department, Georgia Institute of Technology, Atlanta.

His main research interests are in the areas of RF MEMS, silicon micromachining technologies and integrated microsystems.

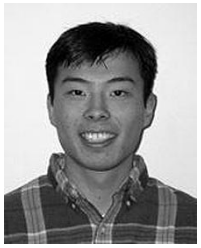

Akinori Hashimura (S'03) was born in 1977 at Nagoya, Japan. In 2000, he received the B.S. degree in electrical engineering from the Georgia Institute of Technology, Atlanta. Following, he continued his education at the Georgia Institute of Technology, where he received the M.S. degree in electrical engineering in 2002.

His research interests were in the areas of MEMS resonators and silicon micromachining technologies. He is currently working for the Panasonic, Osaka, Japan, where he will be continuing his research in the R&D headquarter division.

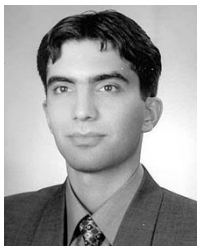

Reza Abdolvand (S'02) was born in Shiraz, Iran, in 1976. He received the B.S. and M.S. degrees in electrical engineering both from Sharif University of Technology, in 1999 and 2001, respectively. He is currently pursuing the Ph.D. degree with the Integrated MEMS group of Georgia Institute of Technology, Atlanta.

His research interests are in the area of MEMS with focus on integrated microresonators.

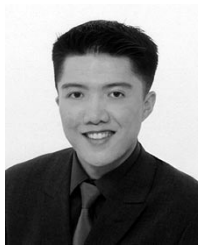

Gavin K. Ho (S'01) was born in Vancouver, Canada, in 1980. He received the M.Eng. degree and B.A.Sc. degree with distinction in mechanical engineering (electromechanical design option) from the University of British Columbia, Canada, in 2001. Following, he joined the Georgia Institute of Technology, Atlanta, where he is currently pursuing the Ph.D. degree in the School of Electrical and Computer Engineering.

His research interests include the physics of loss mechanisms in MEMS resonators and MEMS resonator design for signal processing applications.

Mr. Ho was the recipient of the UBC Letson Prize in 2001 and the Col. Oscar P. Cleaver Award from the Georgia Institute of Technology in 2002.

Ahmet Erbil received the Ph.D. degree in physics from Massachusetts Institute of Technology, Cambridge, in 1983.

After two years at IBM Thomas J. Watson Research Center, Yorktown Heights, NY, he joined Georgia Institute of Technology, Atlanta, Faculty to establish a program on electronic and photonic materials. He has been a Sloan Research Fellow and a recipient of IBM Faculty Development Award. He was a Visiting Professor at Ecole Polytechnique Federale de Lausanne, Switzerland, in fall 1991. He has been consultant to several large industrial firms. He has also been principal investigator on more than 20 projects sponsored by government agencies and corporations. He holds five patents in the field of MOCVD chemicals and thin film production.

Farrokh Ayazi (S'96–M'99) was born on February 19, 1972. He received the B.S. degree in electrical engineering from the University of Tehran, Iran, in 1994 and the M.S. and the Ph.D. degrees in electrical engineering from the University of Michigan, Ann Arbor, in 1997 and 2000, respectively.

He joined the faculty of Georgia Institute of Technology in December 1999, where he is currently an assistant professor in the School of Electrical and Computer Engineering. His current research interests are in the areas of integrated MEMS, RF MEMS, VLSI analog integrated circuits, integrated microsystems, MEMS inertial sensors, and microfabrication technologies.

Prof. Ayazi is the recipient of the Georgia Tech College of Engineering Cutting Edge Research Award for 2001–2002. He received a Rackham Predoctoral Fellowship from the University of Michigan for 1998–1999.